micromachines

Article

A Novel Compliant Connection Mechanism with Thermal Distortion Self-Elimination Function

Yunyang Huang [1], Zhanchen Liao [1], Zhihang Lin [1,*], Fahui Feng [1] and Hui Tang [2,*]

[1] State Key Laboratory of Precision Electronic Manufacturing Technology and Equipment, Guangdong University of Technology, Guangzhou 510006, China; 3121000479@mail2.gdut.edu.cn (Y.H.); 3121000168@mail2.gdut.edu.cn (Z.L.); 3120000440@mail2.gdut.edu.cn (F.F.)
[2] School of Engineering, University of Warwick, Coventry CV4 7AL, UK
* Correspondence: lzh_hi@gdut.edu.cn (Z.L.); huitang@gdut.edu.cn (H.T.)

Abstract: As a novel technology for fabricating large-screen OLED devices, OLED inkjet printing places extreme demands on the positioning accuracy of inkjet printing platforms. However, thermal deformation of the connection mechanism often reduces the printing precision of OLED printing equipment, significantly impacting overall print quality. This study introduces a compliant connection mechanism that achieves precise positioning of the inkjet printing platform and can self-eliminate thermal distortion. The design of the mechanism's core component is based on the Freedom and Constraint Topology (FACT) principle. This component is constructed from three distinct compliant sections arranged in series, collectively providing three degrees of freedom. Furthermore, the resistance to deformation caused by gravity and other external forces was evaluated by analyzing both vertical and horizontal stiffness. To validate the mechanism's thermal distortion elimination and gravity resistance capabilities, finite element analysis (FEA) was carried out. The results demonstrate that the mechanism effectively reduces the maximum deformation of the platform by approximately 46% and the average deformation across the entire platform by approximately 59%. These findings confirm that the mechanism has potential in high-precision positioning tasks that need to mitigate thermal distortion.

Keywords: compliant mechanism; FACT; thermal distortion; OLED inkjet printing

check for updates

Citation: Huang, Y.; Liao, Z.; Lin, Z.; Feng, F.; Tang, H. A Novel Compliant Connection Mechanism with Thermal Distortion Self-Elimination Function. *Micromachines* **2024**, *15*, 774. https://doi.org/10.3390/mi15060774

Academic Editor: Micky Rakotondrabe

Received: 16 March 2024
Revised: 3 June 2024
Accepted: 6 June 2024
Published: 11 June 2024

Copyright: © 2024 by the authors. Licensee MDPI, Basel, Switzerland. This article is an open access article distributed under the terms and conditions of the Creative Commons Attribution (CC BY) license (https://creativecommons.org/licenses/by/4.0/).

1. Introduction

Advances in display technology have led to a growing demand for display devices, with organic light-emitting diodes (OLEDs) being among the most promising candidates. However, the production of large-scale OLED screens is currently constrained by the high costs associated with fine metal mask (FMM) technology [1]. Inkjet printing technology has emerged as a viable solution to this problem, offering several advantages over FMM technology, such as higher material utilization and the flexibility to produce screens of various sizes [2–5].

Inkjet printing stands out due to its efficient material utilization and adaptability to various screen sizes. One of the key factors influencing the performance of inkjet printing devices is the precise positioning of liquid droplets. This accuracy heavily depends on the positioning and movement precision of the mechanical displacement platform as shown in Figure 1.

Currently, inkjet printing equipment relies on high-precision air-bearing motion platforms for positioning and movement. However, these platforms have stringent requirements regarding the surrounding gas, ambient temperature, and equipment temperature [6,7]. Consequently, their high cost and strict usage conditions have limited their widespread application in large-scale OLED screen production.

To address these issues, researchers need to propose a cost-effective connection mechanism to replace the air-bearing motion platform, aiming to achieve the stable and precise

fixation and positioning of the printing platform while minimizing the need for complex equipment and specialized environmental conditions.

Considering these issues, compliant connection mechanisms have been proposed to align the printing platform and mitigate the adverse effects of temperature rises. Compliant connection mechanisms offer frictionless operation, precision, and durability, making them a common choice in robotics manufacturing and precision instrument applications [8–11].

Despite significant progress in compliant mechanisms since the pioneering works of Larry L. Howell [8,9], designing such mechanisms remains challenging for engineers. This paper proposes a novel compliant mechanism utilizing theFACT (Freedom and Constraint Topology) method [12–20]. Firstly, the design principle of this mechanism is introduced. Then, through mechanical and mathematical modeling, the mechanism's thermal deformation absorption capabilities are quantified, establishing vertical and horizontal stiffness models to assess the influence of gravity and other forces.Additionally, to validate the proposed model and conclusions, the finite element method is employed. Finally, the results confirm the effectiveness of our stiffness models in meeting the desired standards and demonstrate the mechanism's remarkable ability to self-compensate for thermal distortions.

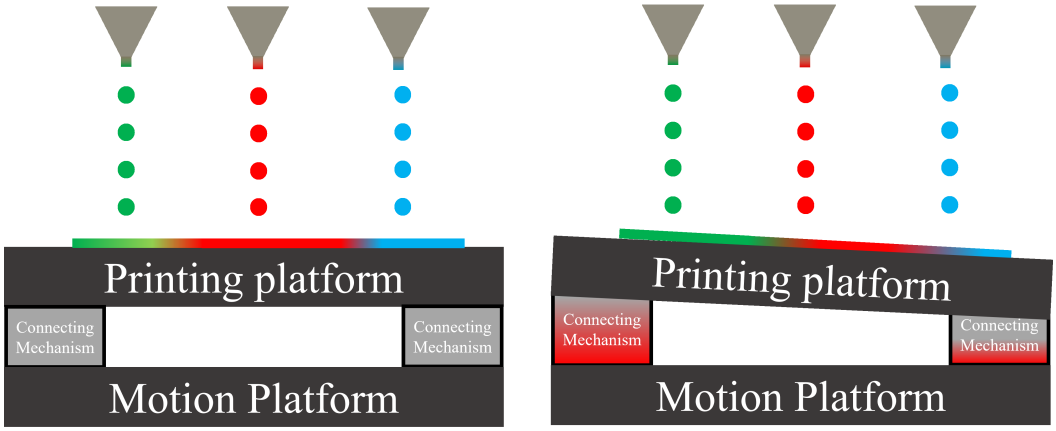


Figure 1. OLED inkjet printing equipment working diagram.

2. Design Principle of Mechanism

Our goal is to create constraints using the principles of exact constraints. These constraints serve to keep the printing platform in a fixed position, preventing any movement between it and the motion platform (Figure 1). Figure 2 illustrates how we will use these constraints to limit the platform's movement to six degrees of freedom in space. To achieve this, we will designate each constraint on each side of the platform as a separate constraint space. Our ultimate aim is to use this constraint space to design compliant mechanisms.

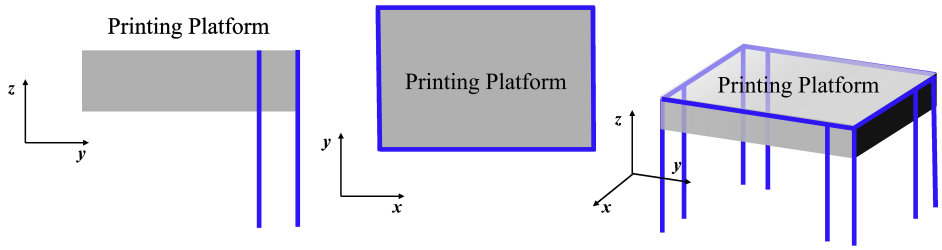


Figure 2. The constraint diagram of the printing platform (the blue line is the constraint line).

The FACT method is a useful tool for visualizing the constraint space by mapping it to the degree of freedom (DOF) space. This method is described in several articles, including [12–18]. The resulting visualization is shown in Figure 3. By applying the principle of FACT, we can deduce that if our mechanism has a freedom space as shown in Figure 3, then it must also have a constraint space as shown in Figure 3 [13].

Notch-type pivots with lumped compliance are commonly used to provide bending and rotation movements, but they have some limitations. For example, they typically have high rotational stiffness, limited stroke length, and high concentrated stress [21–23]. These drawbacks restrict their application in high-precision positioning tasks. To overcome these limitations, this study adopts leaf-type pivots with distributed compliance as the primary component of the design.

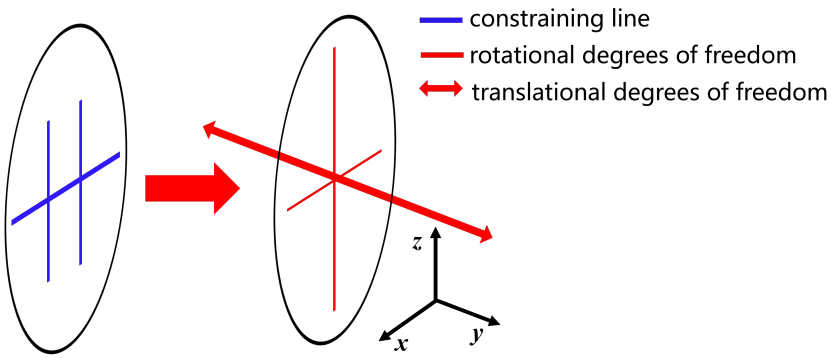


Figure 3. Mapping from constraint space to freedom space.

2.1. Design of Compliant Translation Module

As described in [13], the compliant translation module aims to enable translational movement while restricting other degrees of freedom. To achieve this, we have designed a constraint space and subsequent compliant translational motion module, which is illustrated in Figure 4.

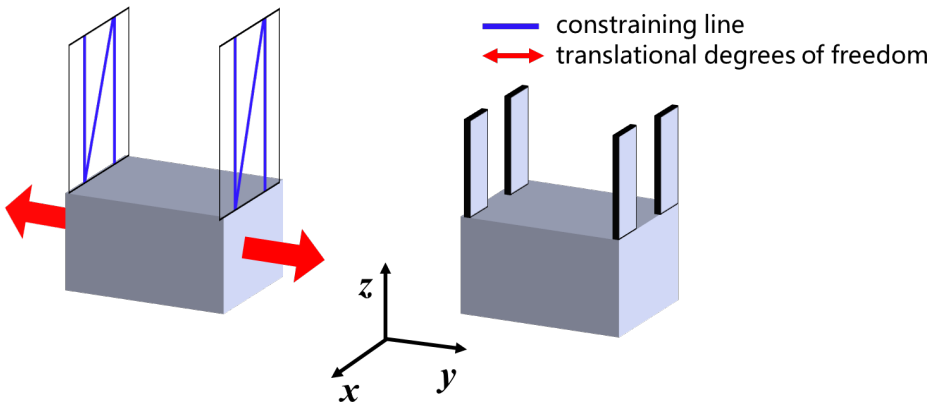


Figure 4. Design flow of compliant translating module.

2.2. Design of Compliant Rotary Motion Module

To achieve two degrees of freedom in the rotational space, we need two separate compliant rotational motion modules placed in series, each for its respective degree of freedom. The design of the rotational DOF (Domain Of Freedom) module is fundamental to the mechanism's overall design. Similar to the design of the compliant translation module, we need to create a corresponding constraint space first as shown in Figure 5. The distribution of this constraint space is vital to ensure the mechanism's efficiency and performance.

To achieve rotational movement around the *X*-axis, a cross-axis flexural pivot can be used. This type of pivot has been extensively studied and modeled in previous research as cited in [11,22,24]. For this particular study, we selected this compliant module to provide rotational freedom around the *X*-axis.

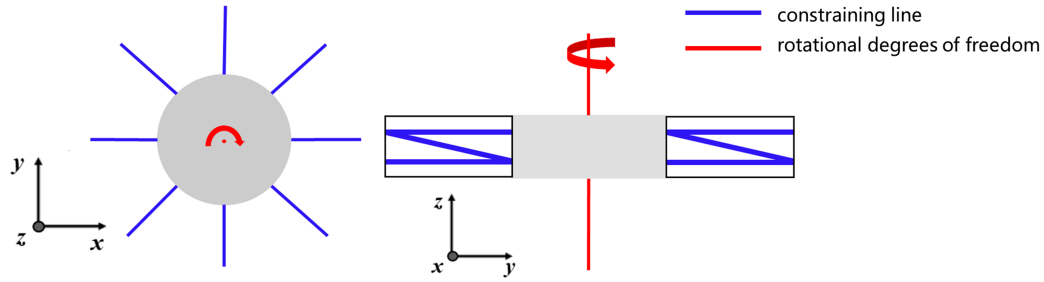


Figure 5. The constraint space design of the compliant rotating module.

2.3. Series Connection and Assembly of Modules

Once all the modules have been designed, it is crucial to inspect the assembly relationship between them. Figure 6 provides a visual representation of this relationship.

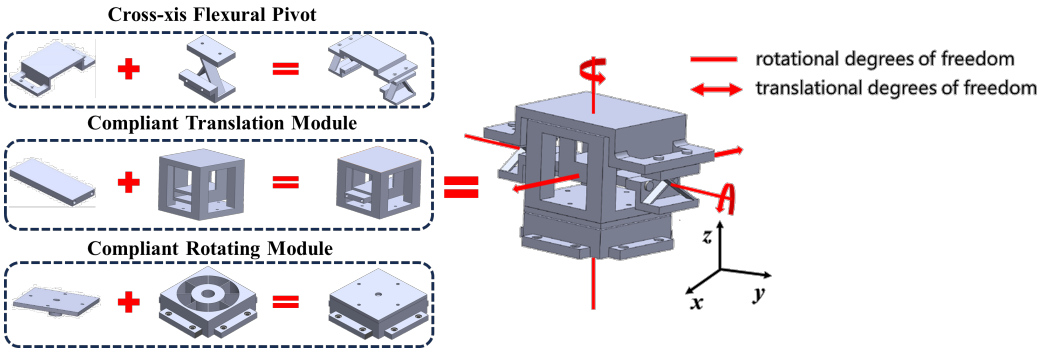


Figure 6. Schematic diagram of assembly relationship between modules and mechanism.

3. Modeling of Compliant Mechanism

In the context of compliant mechanisms, it is important to consider the principle of self-elimination of thermal distortion. When compliant translation mechanisms or compliant rotation mechanisms are exposed to heat, they will deform accordingly. Due to their significantly lower stiffness in a particular direction compared to other directions, thermal deformation tends to occur in that direction. However, the deformation mode shown in Figure 7 does not negatively affect the accuracy of the positioning or motion of the upper platform. Therefore, this mechanism can be considered a self-elimination mechanism for thermal distortion.

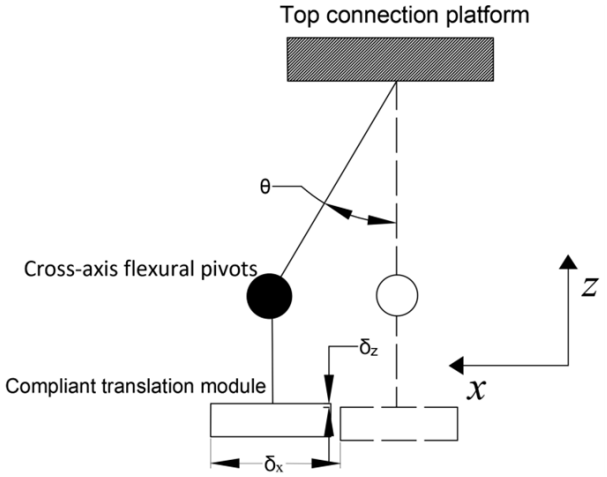


Figure 7. Schematic of deformation of both compliant translation module and cross-axis flexural pivot to absorb thermal stress.

The compliant translational module and the cross-axis flexural pivot's rotational and translational stiffness are significant parameters to evaluate the mechanism's capability to dissipate thermal stress. When the motion stiffness of these components decreases, it indicates that the mechanism can better absorb thermal deformation.

3.1. Modeling of Compliant Translation Module

Due to the challenges in achieving accurate modeling using the rigid body model (RBM), the beam constraint model (BCM) is often used to complete the modeling of bending-compliant parts [25]. In the compliant translation module, we used BCM to complete the construction. For example, we can examine the stress diagram of an ordinary beam in Figure 8 and obtain the equations for the beam's displacements and loads as shown in Equation (1):

$$\begin{bmatrix} f \\ m \end{bmatrix} = \begin{bmatrix} k_{11}^{(0)} & k_{12}^{(0)} \\ k_{12}^{(0)} & k_{22}^{(0)} \end{bmatrix} \begin{bmatrix} y \\ \theta \end{bmatrix} + P \begin{bmatrix} k_{11}^{(1)} & k_{12}^{(1)} \\ k_{12}^{(1)} & k_{22}^{(1)} \end{bmatrix} \begin{bmatrix} y \\ \theta \end{bmatrix} \tag{1}$$

where

$$f = \frac{F_y L^2}{EI_{zz}} \quad m = \frac{ML}{EI_{zz}} \quad p = \frac{PL^2}{EI_{zz}} \tag{2}$$

$$y = \frac{U_y}{L} \quad x = \frac{U_x}{L} \tag{3}$$

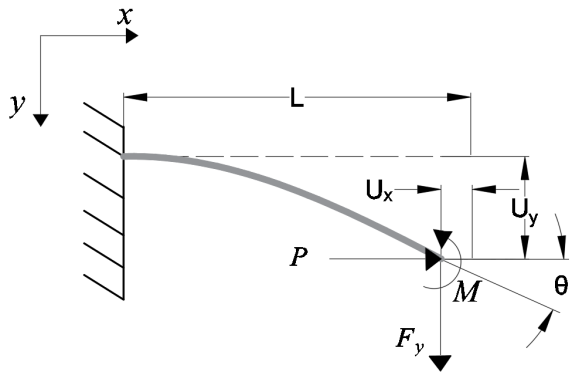


Figure 8. A schematic diagram of a common beam.

However, the mounting platform in the compliant translation module is subjected to two beam forces on one side. The forces are shown in Figure 9.

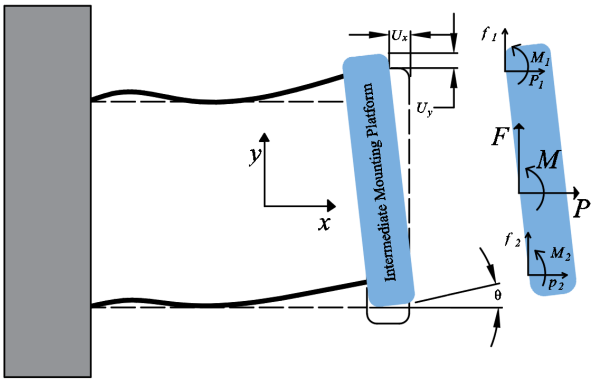


Figure 9. Load and displacement diagram of compliant translation module.

Using the deformation geometry of the two beams:

$$x = \frac{\left(x_1^{k_{11}^{(1)}} + x_2^{k_{11}^{(1)}}\right)}{2} + \frac{\left(x_1^{g_{12}^{(0)}} + x_2^{g_{12}^{(0)}}\right)}{2} \triangleq x^{k_{11}^{(1)}} + x^{g_{12}^{(0)}} \tag{4}$$

$$\omega\theta = \frac{\left(x_2^{k_{11}^{(i)}} - x_1^{k_{11}^{(1)}}\right)}{2} + \frac{\left(x_1^{g_{12}^{(0)}} + x_2^{g_{12}^{(0)}}\right)}{2} \tag{5}$$

$$y_1 = y - \frac{\omega\theta^2}{2} \quad y_2 = y + \frac{\omega\theta^2}{2} \Longrightarrow y_1 \approx y_2 \approx y \tag{6}$$

The characteristic parameters of the beam are in Table 1.

Table 1. The characteristic parameters of the beam.

Parameter	Value	Parameter	Value
$k_{11}^{(0)}$	12	$k_{11}^{(1)}$	1.2
$k_{12}^{(0)}$	−6	$k_{12}^{(1)}$	−0.1
$k_{22}^{(0)}$	4	$k_{22}^{(1)}$	0.13
$g_{12}^{(0)}$	0.5		

We are using a support plate, so we replace the plate modulus with Young's modulus. To obtain the load–displacement equation of the platform, we use the equilibrium relation of the force and moment of the middle installation platform. This results in three equilibrium equations, which are connected with the equation of the deformation geometric relation of the beam. Finally, we solve these equations to obtain the load–displacement equation of the platform:

$$\theta = \frac{\left[4\left(k_{11}^{(0)}\right)^2 + 4P\left(k_{11}^{(1)}k_{11}^{(0)}\right) + P^2\left(k_{11}^{(1)}\right)^2 + f^2 g_{11}^{(1)} d\right]\left[2mk_{11}^{(0)} - 2fk_{12}^{(0)} + P\left(mk_{11}^{(1)} - fk_{12}^{(1)}\right)\right]}{2w^2 d\left(2k_{11}^{(0)} + k_{11}^{(1)}P\right)^3} = \frac{1}{2w^2}\left(t^2 + y^2 g_{11}^{(1)}\right)\left[m - y\left(2k_{11}^{(0)} + pk_{11}^{(1)}\right)\right] \tag{7}$$

$$\begin{aligned} y =& \frac{f - \left(2k_{12}^{(0)} + pk_{12}^{(1)}\right)\theta}{\left(2k_{11}^{(0)} + pk_{11}^{(1)}\right)} = \frac{f}{\left(2k_{11}^{(0)} + pk_{11}^{(1)}\right)} - \frac{\left(2k_{12}^{(0)} + pk_{12}^{(1)}\right)}{2w^2\left(2k_{11}^{(0)} + pk_{11}^{(1)}\right)}\left[t^2 + \frac{f^2 g_{11}^{(1)}}{\left(2k_{11}^{(0)} + pk_{11}^{(1)}\right)^2}\right]\left[m - f\frac{\left(2k_{12}^{(0)} + pk_{12}^{(1)}\right)}{\left(2k_{11}^{(0)} + pk_{11}^{(1)}\right)}\right] \\ \approx& \frac{f}{\left(2k_{11}^{(0)} + pk_{11}^{(1)}\right)} \end{aligned} \tag{8}$$

$$x = \frac{p}{2d} + y^2 i + \frac{p}{2} y^2 g_{11}^{(1)} \tag{9}$$

where

$$p = \frac{\mathrm{PL}^2}{EI_{zZ}} \quad t = \frac{\mathrm{T}}{L} \quad d = \frac{12}{t^2} \tag{10}$$

E_{Izz} represents the moment of inertia for a beam section. To absorb thermal stress, we require low stiffness along the *Y*-axis, and the stiffness *k* is defined as:

$$\frac{1}{k_{f1}} = \frac{y}{f} = \frac{L^3}{EI_{ZZ}2k_{11}^{(0)} + k_{11}^{(1)}P} \tag{11}$$

3.2. Modeling and Analysis of Cross-Axis Flexural Pivot

The analysis of the stiffness of a cross-axis flexural pivot parallels that of a compliant translation mechanism. In this analysis, two supporting beams are modeled as simple beams. The load–displacement relationship at the ends of these beams is determined

using Equation (1). Subsequently, the expression for rotational stiffness is derived from the equilibrium relationship of force and moment on the platform connected by these beams as detailed in Equation (12). These steps are elaborated further in [24]:

$$K_m = \left[\frac{2\left(9\lambda^2 - 9\lambda + 1\right)}{15\cos\alpha} + \lambda\cos\alpha\right] p + 8\left(3\lambda^2 - 3\lambda + 1\right) \tag{12}$$

To effectively absorb thermal stress and deformation, the compliant rotational motion module must work in tandem with the compliant translational motion module to achieve translational motion. Therefore, analyzing the translational stiffness of the compliant rotational motion module is essential:

$$K_{f2} = \frac{K_m}{\lambda\cos\alpha} = \left[\frac{2\left(9\lambda^2 - 9\lambda + 1\right)}{15\lambda\cos^2\alpha} + 1\right] p + \frac{8}{\lambda\cos\alpha}\left(3\lambda^2 - 3\lambda + 1\right) \tag{13}$$

The geometric parameters in Equation (12) and Equation (13) are shown in Figure 10, respectively.

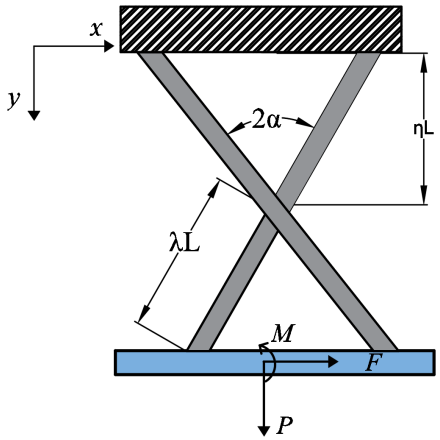


Figure 10. Geometric significance of parameters in cross-axis flexural pivot stiffness analysis.

Since the compliant translational module and the cross-axis flexural pivot are connected in series, the translational stiffness after the combination of the two is

$$K_1 = \frac{K_{f1}K_{f2}}{K_{f1} + K_{f2}} \tag{14}$$

Measuring the rotational stiffness of the compliant translational module is challenging because the rotational angle θ is linked to both the moment m and displacement y. In this case, we estimate the rotational stiffness of the two mechanisms by using the rotational stiffness K_m of the cross-axis flexural pivot.

3.3. Stiffness Modeling in the Vertical Direction

The proposed mechanism has to bear both thermal stress and support the printing platform vertically. We are focusing on examining the stiffness of three compliant mechanisms that are connected in series and are subjected to vertical loads. Based on the beam deflection theory, we have concluded that the cross-axis flexural pivot has a vertical stiffness that remains constant:

$$K_c = \frac{\beta\cos^3\alpha}{v} \tag{15}$$

where

$$\beta = 12\left(\frac{L}{T_p}\right)^2 \quad v = \frac{\eta}{\lambda} \tag{16}$$

where T_p represents the thickness of the beam. In the vertical direction, the two cross-axis flexural pivots are connected in parallel, resulting in a vertical stiffness of $2K_v$ for the cross-axis flexural pivot. Furthermore, the cross-axis flexural pivot, the compliant translation module, and the base are connected in series. Therefore, the formula for calculating the vertical stiffness of the entire mechanism is:

$$K_w = \frac{1}{\frac{1}{k_c} + \frac{1}{k_m} + \frac{1}{k_b}} \tag{17}$$

The vertical stiffness of the compliant translation module when subjected to only vertical forces is:

$$K_m = EA \tag{18}$$

The beams at the base are thick enough in the vertical direction to be considered rigid when subjected to vertical loads from a static perspective. As a result, the vertical stiffness of the final mechanism is:

$$K_v = \frac{EA\beta\cos^3\alpha}{\frac{1}{2}EAv + \beta\cos^3\alpha} \tag{19}$$

3.4. Stiffness Modeling in the Horizontal Direction

In Figure 7, we need the mechanism to provide greater stiffness in the Y-direction to ensure that the top of the rotating mechanism does not move when the compliant translation module is heated and translated. We believe that the mechanism can be considered a rigid body in static analysis if its section moment of inertia along the Y-axis is large enough. In this case, we only need to consider the stiffness of the base on the Y-axis.

When the base is subjected to horizontal force, the deformation of the beam has only two forms—tension and compression. Therefore, we can express the Y-direction stiffness of the base as follows:

$$K_b = \sum_{i=1}^{n} EA|\cos\theta_i| \tag{20}$$

where $\cos\theta_i$ is the angle between the beam and the Y axis, and n is the number of beams. Since all beams are parallel to each other, the stiffness of the entire mechanism in the Y-axis direction is equal to the sum of the components of all the beams in the Y-axis direction. After completing the modeling analysis of the mechanism, we need to determine the optimal design size using the formula obtained from the modeling.

4. Determination of Mechanism Size

We need to ensure that the mechanism has the maximum stiffness in the constraint direction and the minimum stiffness in the direction of the degree of freedom so that the mechanism can better absorb the thermal stress. In mathematical terms,

$$\text{Max}\{K_b, K_v\} \tag{21}$$

$$\text{Min}\{K_1, K_m\} \tag{22}$$

After understanding some basic optimization objectives and constraints, we determine the geometric parameters that need to be optimized. They are in the cross-axis flexural pivot: λ, L, α, and cross-sectional size of the beam: a length a and a width b (the width b needs to be three or more times the length a). The compliant translation mechanism can be designed separately from the cross-axis flexural pivot module, so we need to optimize L_2, a_2, and b_2 of the compliant translation module. Due to the large number of parameters to be optimized and the wide range of optimization options, we decided to use the Monte Carlo algorithm to estimate the optimal size model under the constraints. Set the expression of the objective function:

$$\text{Max}\, K = \omega_1 K_b + \omega_2 K_v - \omega_3 K_1 - \omega_4 K_m. \tag{23}$$

where $\omega_i (i = 1, 2, 3, 4)$ is the weight. Build the code and model in Matlab (Matlab version 2020b), set the appropriate number of Monte Carlo samples, and then solve it to obtain a maximum value of the objective function. Under the condition of the maximum value of the objective function, the final size of the mechanism is determined as Table 2.

Table 2. Optimal size values of mechanism

Parameter	Value	Parameter	Value
λ	12	α	0.61
L	14.6 mm	a	0.8 mm
b	3.6 mm	L_1	7.9 mm
a_1	0.6 mm	b_1	2.1 mm

5. Simulation Verification

Steady-state thermal, static structure, and modal analysis was conducted on assemblies using ANSYS 19.2. The temperature of the moving platform at the bottom was set to 200 °C to simulate working conditions. The main objective was to evaluate the deformation error of the printing platform caused by thermal deformation of the connecting parts due to temperature increase. The results, shown in Figures 11–13, indicate that the traditional rigid connection is superior to the present method.

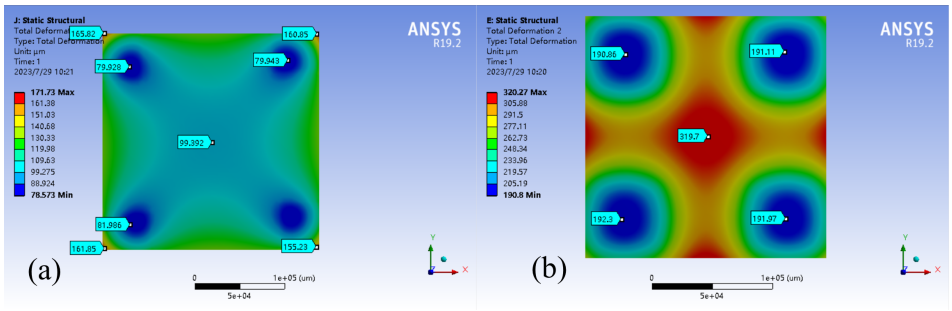


Figure 11. Thermal deformation of the printing platform. (**a**) With the compliant connector; (**b**) Without the compliant connector.

The results of the finite element analysis conducted at a temperature of 200 °C indicate that using a compliant connection module for the printing platform significantly reduced thermal deformation compared to traditional rigid connections. The maximum deformation decreased from 320 µm to 170 µm, a 46% reduction. Additionally, the average deformation decreased from 260 µm to 107 µm, representing a 59% reduction. The deformation shifted from the middle of the sensitive part of the printing platform to the non-sensitive corners. Furthermore, the maximum temperature of the printing platform was reduced from 180 °C to 80 °C, resulting in a 45% reduction.

The modal analysis revealed that the first two natural frequencies of the mechanism are closely identical (441.11 Hz and 441.13 Hz). This implies that the mechanism exhibits similar vibration characteristics in these two modes, suggesting that their vibrations may interact, leading to more complex vibrations. We discovered that the vibration modes of the printing platform exhibit high stiffness at various vibration frequencies, suggesting that these frequencies have a high degree of rigidity and are resistant to deformation.

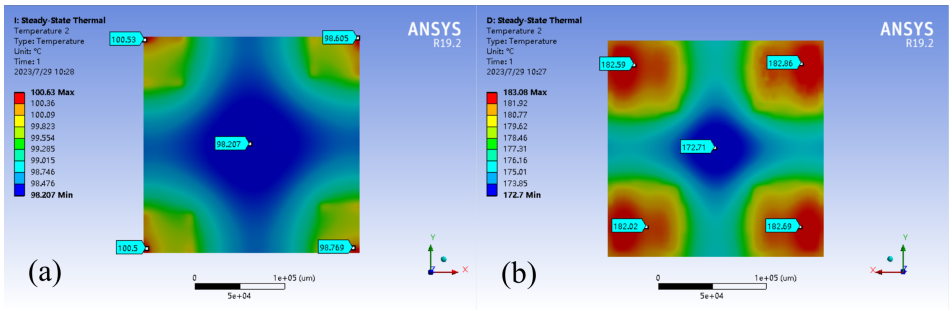


Figure 12. Temperature of the print platform at thermal equilibrium. (**a**) With the compliant connector; (**b**) Without the compliant connector.

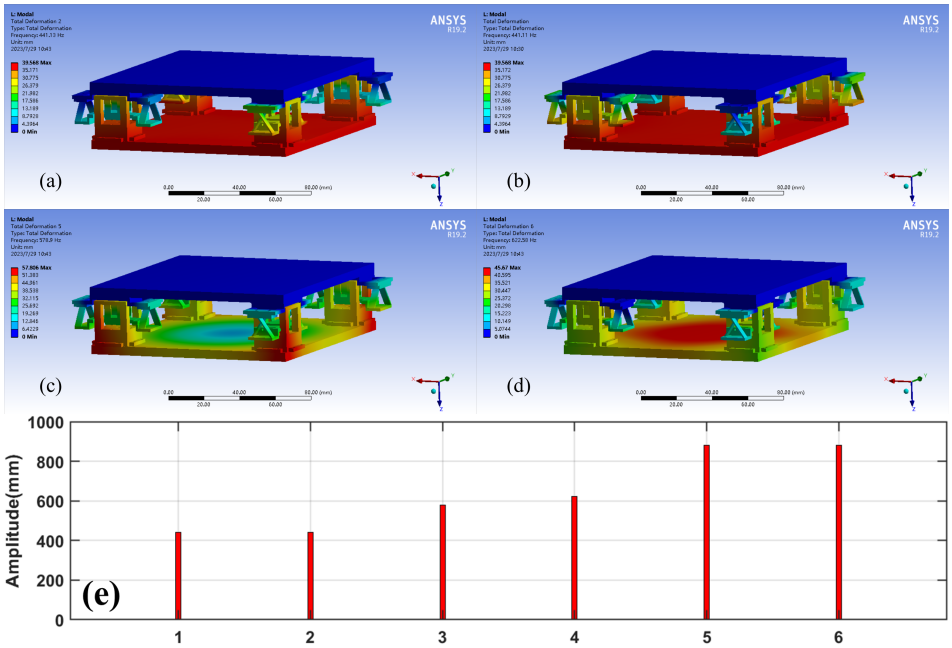


Figure 13. Natural frequencies of the proposed mechanism. (**a**) 1st; (**b**) 2nd; (**c**) 3rd; (**d**) 4th; (**e**) 6 orders.

6. Conclusions

This paper introduces a novel compliant connection mechanism based on the FACT method, aimed at enhancing the performance of OLED inkjet printing devices. The mechanism addresses issues such as misalignment caused by thermal deformation in OLED inkjet printing devices.We developed static and dynamic models for the mechanism, providing force–displacement expressions for the mechanism. With the objectives of maximizing support stiffness and maximizing thermal deformation absorption capacity, we optimized the size of the mechanism using the obtained mathematical model expressions. Finally, we conducted finite element analysis to validate the mechanism. The results indicate that the maximum thermal deformation of the printing platform connected by the compliant connection mechanism is reduced by 46% compared to traditional rigid connections, decreasing from 320 μm to 170 μm. Additionally, the average deformation of the printing platform is reduced by 59%, from 260 μm to 107 μm, compared to traditional rigid connections. This demonstrates the effectiveness of the compliant connection mechanism in reducing thermal distortion. These results meet our design requirements and offer a potential solution for OLED inkjet printing equipment.

Author Contributions: Y.H. conceived the idea and designed the structure. Y.H. and Z.L. (Zhanchen Liao) complete the theoretical analysis. Y.H., Z.L. (Zhanchen Liao), F.F. and H.T. contributed to data analysis and interpretation. Y.H. and Z.L. (Zhihang Lin). wrote the paper and all authors provided feedback. All authors have read and agreed to the published version of the manuscript.

Funding: This research was funded by the Natural Science Foundation of China under Grant 52305597, Science and Technology Projects in Guangzhou under Grant SL2022A04J01372, and funded by State Key Laboratory of Precision Electronic Manufacturing Technology and Equipment under Grant JMDZ202313, in part by the European Unions Horizon 2020 research and innovation programme under the Marie Sklodowska-Curie Grant agreement no. 101026104, Engineering Technology Center of Guangdong General University under Grant 2022GCZX005.

Data Availability Statement: The original contributions presented in the study are included in the article, further inquiries can be directed to the corresponding authors.

Conflicts of Interest: The authors declare no conflicts of interest.

References

1. Wang, S.; Zhang, H.; Zhang, B.; Xie, Z.; Wong, W.Y. Towards high-power-efficiency solution-processed OLEDs: Material and device perspectives. *Mater. Sci. Eng. R Rep.* **2020**, *140*, 100547. [CrossRef]
2. Madigan, C.F.; Hauf, C.R.; Barkley, L.D.; Harjee, N.; Vronsky, E.; Van Slyke, S.A. 30.2: Invited paper: Advancements in inkjet printing for OLED mass production. In Proceedings of the SID Symposium Digest of Technical Papers, San Diego, CA, USA, 1–6 June 2014; Volume 45, pp. 399–402.
3. Gassend, V.; Hauf, C.R.; Chen, J. 33-3: Invited Paper: Research and Applications of Inkjet Printing for OLED Mass Production. In Proceedings of the SID Symposium Digest of Technical Papers, San Jose, CA, USA, 8–13 August 2022; Volume 53, pp. 398–401.
4. Levermore, P.; Schenk, T.; Tseng, H.R.; Wang, H.J.; Heil, H.; Jatsch, A.; Buchholz, H.; Böhm, E. 38-1: Invited Paper: Ink-jet-printed OLEDs for display applications. In Proceedings of the SID Symposium Digest of Technical Papers, San Francisco, CA, USA, 22–27 May 2016; Volume 47, pp. 484–486.
5. Villani, F.; Vacca, P.; Nenna, G.; Valentino, O.; Burrasca, G.; Fasolino, T.; Minarini, C.; Della Sala, D. Inkjet printed polymer layer on flexible substrate for OLED applications. *J. Phys. Chem. C* **2009**, *113*, 13398–13402. [CrossRef]
6. Ro, S.K.; Kim, S.; Kwak, Y.; Park, C.H. A linear air bearing stage with active magnetic preloads for ultraprecise straight motion. *Precis. Eng.* **2010**, *34*, 186–194. [CrossRef]
7. Zhang, F.; Liu, P. Accuracy improvement of the H-drive air-levitating wafer inspection stage based on error analysis and compensation. *Meas. Sci. Technol.* **2018**, *29*, 045013. [CrossRef]
8. Howell, L.L.; Magleby, S.P.; Olsen, B.M.; Wiley, J. *Handbook of Compliant Mechanisms*; Wiley Online Library: Hoboken, NJ, USA, 2013.
9. Howell, L.L. Compliant mechanisms. In Proceedings of the 21st Century Kinematics: The 2012 NSF Workshop, Chicago, IL, USA, 11–12 August 2012; pp. 189–216.
10. Jia, Y.; Tang, H.; Xu, S.; Xu, Y.; Chen, X.; Tian, Y. A novel decoupled flexure nanopositioner with thermal distortion self-elimination function. *IEEE/ASME Trans. Mechatron.* **2021**, *27*, 2953–2962. [CrossRef]
11. Zhu, Z.; Tang, H.; Huang, Y.; Lin, Z.; Tian, Y.; Yu, P.; Su, C. A compliant self-stabilization nanopositioning device with modified active—Passive hybrid vibration isolation strategy. *IEEE/ASME Trans. Mechatron.* **2023**, *28*, 3305–3316. [CrossRef]
12. Hopkins, J.B.; Culpepper, M.L. Synthesis of multi-degree of freedom, parallel flexure system concepts via Freedom and Constraint Topology (FACT)–Part I: Principles. *Precis. Eng.* **2010**, *34*, 259–270. [CrossRef]
13. Hopkins, J.B.; Culpepper, M.L. Synthesis of multi-degree of freedom, parallel flexure system concepts via freedom and constraint topology (FACT). Part II: Practice. *Precis. Eng.* **2010**, *34*, 271–278. [CrossRef]
14. Hopkins, J.B.; Culpepper, M.L. Synthesis of Multi-Degree-of-Freedom Precision Flexure Concepts via Freedom and Constraint Topologies. In Proceedings of the American Society for Precision Engineering, Dallas, TX, USA, 14–19 October 2007.
15. Hopkins, J.B. Design of Flexure-Based Motion Stages for Mechatronic Systems via Freedom, Actuation and Constraint Topologies (FACT). Ph.D. Thesis, Massachusetts Institute of Technology, Cambridge, MA, USA, 2010.
16. Hopkins, J.B. Design of Parallel Flexure Systems via Freedom and Constraint Topologies (FACT). Ph.D. Thesis, Massachusetts Institute of Technology, Cambridge, MA, USA, 2007.
17. Li, S.; Yu, J.; Pei, X.a.; Su, H.j.; Hopkins, J.B.; Culpepper, M. Type Synthesis Principle and Practice of Flexure Systems in the Framework of Screw Theory: Part III—Numerations and Synthesis of Flexure Mechanisms. In Proceedings of the International Design Engineering Technical Conferences and Computers and Information in Engineering Conference, Montreal, QC, Canada, 15–18 August 2010; Volume 44106, pp. 619–628.
18. Li, L.; Zhang, D.; Guo, S.; Qu, H. Design, modeling, and analysis of hybrid flexure hinges. *Mech. Mach. Theory* **2019**, *131*, 300–316. [CrossRef]
19. Yu, X.; Zhou, J.; Liang, H.; Jiang, Z.; Wu, L. Mechanical metamaterials associated with stiffness, rigidity and compressibility: A brief review. *Prog. Mater. Sci.* **2018**, *94*, 114–173. [CrossRef]

20. Kaminakis, N.T.; Stavroulakis, G.E. Topology optimization for compliant mechanisms, using evolutionary-hybrid algorithms and application to the design of auxetic materials. *Compos. Part B Eng.* **2012**, *43*, 2655–2668. [CrossRef]
21. Tang, H.; Li, J.; Jia, Y.; Gao, J.; Li, Y. Development and testing of a large-stroke nanopositioning stage with linear active disturbance rejection controller. *IEEE Trans. Autom. Sci. Eng.* **2021**, *19*, 2461–2470. [CrossRef]
22. Tang, H.; He, S.; Zhu, Z.; Gao, J.; Zhang, L.; Cui, C.; Chen, X. A monolithic force sensing integrated flexure bonder dedicated to flip-chip active soft-landing interconnection. *IEEE/ASME Trans. Mechatron.* **2020**, *26*, 323–334. [CrossRef]
23. Huo, T.; Yu, J.; Zhao, H. Design of a kinematic flexure mount for precision instruments based on stiffness characteristics of flexural pivot. *Mech. Mach. Theory* **2020**, *150*, 103868. [CrossRef]
24. Awtar, S.; Slocum, A.H.; Sevincer, E. Characteristics of beam-based flexure modules. *J. Mech. Des.* **2007**, *129*, 625–639. [CrossRef]
25. Zhao, H.; Bi, S.; Yu, J. Nonlinear deformation behavior of a beam-based flexural pivot with monolithic arrangement. *Precis. Eng.* **2011**, *35*, 369–382. [CrossRef]

Disclaimer/Publisher's Note: The statements, opinions and data contained in all publications are solely those of the individual author(s) and contributor(s) and not of MDPI and/or the editor(s). MDPI and/or the editor(s) disclaim responsibility for any injury to people or property resulting from any ideas, methods, instructions or products referred to in the content.